

論文 / 著書情報  
Article / Book Information

Title	Influence of initial fines content on fabric of soils subjected to internal erosion
Authors	Mao Ouyang, Akihiro Takahashi
Citation	Canadian Geotechnical Journal, Vol. 53, No. 2, pp. 299-313
Pub. date	2016, 2
DOI	<a href="http://dx.doi.org/10.1139/cgj-2014-0344">http://dx.doi.org/10.1139/cgj-2014-0344</a>
Note	This file is author (final) version.

1 Influence of initial fines content on fabric of soils subjected to  
2 internal erosion

3  
4  
5 Mao Ouyang, Akihiro Takahashi

6  
7 **M. Ouyang.** Department of Civil Engineering, Tokyo Institute of Technology, 2-12-1-M1-3 Oh-  
8 okayama, Meguro, Tokyo 152-8552, Japan. (e-mail: ouyang.m.aa@m.titech.ac.jp)

9 **A. Takahashi.** Department of Civil Engineering, Tokyo Institute of Technology, 2-12-1-M1-3 Oh-  
10 okayama, Meguro, Tokyo 152-8552, Japan. (e-mail: takihiro@cv.titech.ac.jp)

11  
12  
13 **Corresponding author:** Akihiro Takahashi (e-mail: takihiro@cv.titech.ac.jp)

14  
15 **Canadian Geotechnical Journal, 53(2), 299-313, 2016**

16 **Original URL:**

17 **<http://dx.doi.org/10.1139/cgj-2014-0344>**

18

19 **Abstract:** Seepage-induced internal erosion often happens in earth structures. This paper presents  
20 experimental investigations on the influence of initial fines content on fabric of soils subjected to  
21 internal erosion. The tested materials were the binary mixtures of silica No. 3 and silica No. 8, which  
22 correspond to the coarse and fine fractions, respectively. One group of specimens was prepared with  
23 initial fines contents of 0, 15%, 25%, and 35% by weight. The undrained monotonic compression tests  
24 were performed on this group to examine the influence of fines content on the undrained behavior. The  
25 other group was prepared with initial fines contents of 15%, 25%, and 35% by weight, on which the  
26 seepage tests and subsequent undrained compression tests were carried out to demonstrate the  
27 mechanical influence of the internal erosion. The undrained behavior of the first group of specimens  
28 reveals that the presence of fines would decrease the peak and residual strengths. A comparison  
29 between the undrained behavior of soils with erosion and that of soils without erosion shows that the  
30 soils become less contractive after the internal erosion. When the axial strain is less than 0.4%, the  
31 undrained secant stiffness of soils with erosion is larger than that without erosion at the same axial  
32 strain. Meanwhile, the undrained peak strength and residual strength are larger for soils with erosion  
33 than that for soils without erosion. The less amount of excess pore -water pressure is generated during  
34 the undrained compression for the eroded soils comparing to those of the uneroded soils. Furthermore,  
35 the eroded soils show a wider instability zone than that of the uneroded soils, which suggests that the  
36 instability zone be enlarged by the internal erosion. Besides, one-dimensional upward seepage tests  
37 were performed to investigate the change of fabric of the mixed sand with 15%, 25%, and 35% fines  
38 contents due to internal erosion. The recorded microscopic images of soils before and after erosion  
39 reveal that the fabric is altered by the internal erosion.

40

41 *Key words:* fines content, internal erosion, undrained compression, soil strength

42

43 **Introduction**

44

45 Internal erosion is a subsequent transport of detached finer soil particles through the matrix under  
46 seepage flow. The initiation of internal erosion has been investigated in terms of the susceptibility of  
47 material, hydraulics, and mechanics (Bonelli 2012). However, there were only few researches on the  
48 mechanical consequences of soil subjected to internal erosion from the viewpoint of fabric (Moffat and  
49 Fannin 2011; Moffat et al. 2011). The fabric here represents the composition of soil, the spatial  
50 arrangement of particles, particle groups, and pore spaces (Mitchell and Soga 2005). This fabric may  
51 be affected by fines content and specimen preparation method for the soil testing on reconstituted  
52 specimens.

53

54 Internal erosion causes physical and mechanical changes in soil in many ways. Ke and Takahashi  
55 (2012, 2014b) conducted seepage tests in a column and a triaxial permeameter, respectively, and  
56 observed that internal erosion would trigger the deformation of tested soils and consequently result in  
57 the alteration of soil strength. Moreover, that amounts of deformation and soil strength change were  
58 related with the assigned hydraulic conditions (i.e., imposed hydraulic gradient or Darcy velocity).  
59 Coincident with the experimental investigations, several novel models for internal erosion had been  
60 proposed. Based on the laboratory experiments performed by Sterpi (2003), the empirical law had been  
61 derived to describe the process of erosion, in which the amount of eroded soil was considered as a  
62 function of time and of the hydraulic gradient. By adopting that erosion law, Cividini and Gioda (2004)  
63 proposed a finite element approach in analyzing the transportation of fines. To estimate the quantity of  
64 eroded soil mass induced by internal erosion and the resulting settlement of shallows foundations in the  
65 city of Milan, Cividini et al. (2009) improved that erosion law in the rate form, and accordingly  
66 performed finite element simulations. It was indicated that the erodible fines showed an upper limit  
67 diameter of 0.074 mm. The transportation of these fines by seepage flow led to a decline in soil density

68 and a settlement of nearby buildings. Besides, the multi-scale approaches were applied to simulate the  
69 process of internal erosion and to examine the mechanical consequences by Scholtès et al. (2010). It  
70 was elaborated that the internal erosion tended to increase the porosity, which led to a decrease of the  
71 angle of shearing resistance. Muir Wood et al. (2010) simulated internal erosion by discrete element  
72 method (DEM) and concluded that the change of the grading by the extraction of fines would cause a  
73 change of the critical state in the effective stress plane, resulting in a change of soil strength.

74

75 Figure 1 shows the schematic diagram of typical behaviors of granular soils in the undrained  
76 compression test. Here the shear stress is defined as the difference between the axial and radial stresses.  
77 The undrained peak state (A and A' in Fig. 1) is a state where shear stress reaches an initial local  
78 maximum value in the stress–strain curve, quasi-steady state (B and B' in Fig. 1) is where the shear  
79 stress reaches a minimum value (Alarcon-Guzman et al. 1988). Phase transformation state (C in Fig. 1)  
80 is an indication that soil behavior changes from contractive to dilative. The points D and D' stand for  
81 the critical state, which represents the ultimate condition where the plastic shearing could continue  
82 indefinitely without changes in volume or effective stress (Muir Wood 1990). When the critical state  
83 coincides with the quasi-steady state, it indicates the occurrence of flow behavior (dashed line in Fig. 1)  
84 (Tsukamoto et al. 2009). The limited flow behavior (solid line in Fig. 1) suggests that the shear stress  
85 temporarily decreases after its initial peak, but reaches a larger value at critical state as shearing  
86 continues.

87

88 Many experiments have been performed on soil mixtures to examine the effects of fines content on the  
89 soil mechanical behavior. Thevanayagam and Mohan (2000) reported that the shear stress at undrained  
90 peak state was smaller for the soil with plastic fines than that for the clean sand at the same void ratio  
91 when the fines content was smaller than 30%. The shear stress at undrained peak state decreased with  
92 an increase in nonplastic fines for Lagunillas sand and Tia Juana sand (Ishihara 1993). Murthy et al.

93 (2007) indicated that the Ottawa sand with nonplastic fines (5%, 10%, and 15%) showed a more  
94 contractive and collapse tendency. Nevada sand with nonplastic fines content (10%, 20%, and 30%)  
95 also showed a more contractive behavior than the clean sand in both drained and undrained monotonic  
96 compression test (Lade and Yamamuro 1997). Meanwhile, Nevada sand with 7% nonplastic fines  
97 showed flow behavior and limited flow behavior at relative small initial confining pressure (Yamamuro  
98 and Covert 2001). A reduction of shear stress at the quasi-steady state caused by an addition of plastic  
99 fines (10% and 20%) was reported by Ni et al. (2004). The instability zone became larger with the  
100 increase in plastic fines content up to 10%, whereas it decreased when the fines content was greater  
101 than 20% (Abedi and Yasrobi 2010). Here the instability zone is defined as the zone between the line  
102 connecting the origin to the undrained peak state and the line connecting the origin to the phase  
103 transformation state in the effective stress plane for cohesionless soil.

104

105 The influence of fines on critical state has been widely studied. Murthy et al. (2007) noted that an  
106 addition of nonplastic fines led to an increase in the angle of shearing resistance. The shear stress at an  
107 axial strain level of 20%–25% decreased with an addition of nonplastic fines to clean Nevada sand  
108 (Thevanayagam, 1998). Ni et al. (2004) manifested that the position of the critical state line (CSL) of  
109 the soil mixture containing plastic fines in the void ratio and mean effective stress plane was greatly  
110 influenced by the stress history, whereas the position of the CSL in the same plane of the soil mixture  
111 containing nonplastic fines was mostly affected by the soil fabric comparing to the stress history.  
112 Rahman et al. (2011) reported that the CSL in the void ratio and mean effective stress plane shifted  
113 downward with an addition of nonplastic fines within the range of threshold fines content. However,  
114 when the fines content was beyond the threshold value, the CSL moved upward with the increase of  
115 fines content.

116

117 The undrained behavior is influenced by the soil preparation method as well. It was observed that the

118 soil prepared by moist tamping method showed a more contractive behavior than that prepared by  
119 water pluviation (Vaid et al. 1990). Yang et al. (2008) noted that the dilative responses dominated for  
120 the soil prepared by moist tamping method comparing to that prepared by dry deposition method.

121

122 This paper describes the results of a laboratory study of undrained behavior of soils with and without  
123 erosion. The focus is to examine the difference of overall undrained behavior at both small strain level  
124 and large strain level of eroded soils and uneroded soils. The undrained peak state is discussed in terms  
125 of peak strength and mean effective stress ratio. Besides, the initial secant stiffness is illustrated.  
126 Changes induced by the internal erosion at quasi-steady state and phase transformation state are  
127 elaborated by interpreting the variance in residual strength and flow potential. The possible reasons for  
128 the changes of the behavior of soils with erosion are demonstrated by the microscopic observation of  
129 the soils before and after the internal erosion. Finally, the correlation between the undrained peak state  
130 and the quasi-steady state, together with that between undrained peak state and the phase  
131 transformation state, is demonstrated.

132

### 133 **Experimental program**

134

#### 135 **Tested materials**

136

137 All the materials in the experiments were mixture of silica No. 3 and No. 8. Individual particle is  
138 subround to subangular in shape and predominant mineral is silica. Silica No. 3 is regarded as coarse  
139 particles, which forms the skeleton of the specimen. Silica No. 8 is treated as fines, which could be  
140 transported by seepage flow. The properties of the individual sand and the mixed sands with 15%, 25%,  
141 and 35% fines contents are shown in Table 1, and the particle-size distribution curves are plotted in Fig.  
142 2. One group of tested specimens was prepared with initial fines contents of 0, 15%, 25%, and 35% by

143 weight. The undrained monotonic compression tests were performed on this group to examine the  
144 influence of initial fines content on the undrained mechanical behavior. Another group of tested  
145 specimens was prepared with 15%, 25%, and 35% initial fines contents, on which the seepage tests and  
146 subsequent undrained compression tests were performed to investigate the effects of internal erosion on  
147 soil behavior. The seepage tests performed on this group of specimens were carried out in a revised  
148 triaxial cell developed by Ke and Takahashi (2014a), which is shown in Fig. 3.

149

### 150 **Test apparatus**

151

152 The main part of the triaxial apparatus is summarized here. The vertical axial load was automatically  
153 applied by the loading system with a motor-gear system, which could compress the tested specimen at  
154 a given strain rate. The cell pressure was applied by the regulated air pressure whose source was  
155 maintained constantly at 700 kPa through an automatic air compressor. A 5 mm thickness mesh with 1  
156 mm openings, which follows the recommendation from the U.S. Department of Agriculture (USDA  
157 1994) to fully hold the coarse particles and allow the erosion of fines, was placed on the end-plate of  
158 the pedestal. The base pedestal was revised to accommodate the seepage tests. The drilled conical  
159 trough and the tube directly connecting the conical trough with the sedimentation tank were designed to  
160 allow the fully dislodgement of fines from the specimens. A miniature load cell in the sedimentation  
161 tank would record the cumulative eroded soil mass during the seepage test.

162

### 163 **Test procedures**

164

165 All the specimens were prepared targeting the same initial relative density ( $D_r = 30\%$ ). The size of the  
166 soil specimens was approximately 70 mm in diameter and 150 mm in height. The moist tamping  
167 method was employed in this study. If each layer is compacted to the target density, the lower portion

168 of the specimen becomes denser than the upper portion because the repeated compaction energy is  
169 applied to the lower portion with succeeding compaction. To avoid this problem, other than the final  
170 layer, each layer was compacted to a lower density than the target density of the whole specimen  
171 according to the undercompaction theory (Ladd 1978). This study adopted Lade's undercompaction  
172 theory, and the soil specimen has been prepared layer by layer with 10 layers in total. To guarantee the  
173 target soil density is actually achieved, the after-test oven-dry weight of the soil specimen has been  
174 checked.

175

176 After the soil preparation, the top cap was attached and fixed on the surface of the specimen. The  
177 vacuum saturation procedure (JGS 2000; ASTM 2012) was adopted in the experiment. Vacuum was  
178 applied to the specimen through water reservoirs gradually until  $-80$  kPa, keeping the pressure  
179 difference inside and outside of the specimen constant at 20 kPa. The de-aired water with a total  
180 volume of about 10 times of the pore volume was slowly injected into the specimens from the bottom.  
181 Generally, the B value of these specimens equals to or is greater than 0.95, which was considered as  
182 saturated specimens in this test. After the saturation, all specimens were isotropically consolidated by  
183 an automatic control system to an initial mean effective stress of 50 kPa.

184

185 The undrained monotonic compression test was performed on one group of specimens containing 0,  
186 15%, 25%, and 35% fines contents with an axial strain rate of 0.1%/min (JGS 2000; ASTM 2012) upon  
187 the completion of consolidation to examine the influence of fines content on the undrained behavior.

188

189 To study the influence of internal erosion on the soil mechanical behavior, seepage test was performed  
190 on the other group of specimens in the triaxial cell after the complete isotropic consolidation. The water  
191 in the seepage tests was supplied by the water reservoir shown in Fig. 3, and it was pumped into the  
192 specimens by the flow pump. The procedure of the application of flow rate is shown in Fig. 4, which is

193 the same as the test conducted by Ke and Takahashi (2014a). At first, the seepage flow was assigned at  
194 a relatively lower flow rate. Then a constant large flow rate ( $5.2 \times 10^{-6} \text{ m}^3/\text{s}$ ) was applied to the  
195 specimen. Upon the completion of the seepage test, the undrained monotonic compression test was  
196 performed on the eroded soils with an axial strain rate of 0.1%/min (JGS 2000; ASTM 2012).

197

## 198 **Test results**

199

### 200 **Seepage test results**

201

202 According to Kenney and Lau (1985), the particles finer than grain size  $d$  would likely to be eroded  
203 from a soil matrix if there were fewer particles in the grain sizes from  $d$  to  $4d$ . In this study, the  
204 mixtures of silica No. 3 and No. 8 were gap-graded soils. Therefore, part of fines would be transported  
205 by the assigned seepage flow and accumulated in the sedimentation tank (Fig. 3). A summary of results  
206 of seepage tests is shown in Table 2. To show the repeatability of test results, seepage tests and  
207 subsequent undrained compression tests were carried out twice on the soils with 25% initial fines  
208 content, corresponding to the specimens 25\_WE\_DR30\_N1 and 25\_WE\_DR30\_N2 (where the first  
209 number in the specimen ID represents percentage of fines content; the second entry is with or without  
210 erosion; the third is relative density percentage; and the fourth is test number). The evolutions of the  
211 cumulative eroded soil mass are shown in Fig. 5. It is noted that the fines are eroded away from the  
212 specimen continuously at the constant flow rate. As the seepage tests were performed on gap-graded  
213 soils under isotropic stress state, it could be assumed that the effective stresses are mainly transferred  
214 by the coarse fractions. Therefore, the intergranular void ratio, defined by regarding the fines as voids,  
215 is considered as one of the parameters in interpreting the relation between initial fines content and  
216 cumulative eroded soil mass. Observations of Table 2 reveal that the intergranular void ratios are  
217 similar for specimens with 15% and 25% initial fines contents before and after seepages tests whilst the

218 specimen with 35% initial fines content shows a reduction of intergranular void ratio after erosion. It  
219 suggests that the fines in these mixtures might not be involved in the stress transformation, which then  
220 results in easier transportation of fines when subjected to certain seepage flow. Therefore, it could be  
221 concluded that the more the initial fines content, the larger the amount of cumulative eroded soil mass  
222 within the scope of this study.

223

224 The median particle size of coarse and fine particle is 1.76 and 1.16 mm (Table 1), respectively. If both  
225 are assumed as spheres, the diameter of the inscribed sphere in the minimum void space formed by  
226 coarse particles is around 0.73 mm. It is approximately five times larger than the median diameter of  
227 fines, which suggests a smaller possibility of the occurrence of clogging of fines. Thus the increase in  
228 the initial fines content does not necessarily reduce the cumulative eroded soil.

229 The soil particles were transported by the water flow, which results in a change of volumetric strain  
230 during the seepage tests. Figure 6 shows the evolution of the volumetric strain during the seepage tests.  
231 There are many jumps in the volumetric strain change for the soil with 35% fines content, which might  
232 be attributed to the sudden erosion of the fines by seepage flow. It is indicated that the volumetric strain  
233 change is related to the initial fines content. The volumetric strain of the soil with 35% initial fines  
234 content (35\_WE\_DR30) is approximately five times larger than the soil with 25% initial fines content  
235 (25\_WE\_DR30\_N1) at the end of the test.

236

### 237 **Undrained compression test results**

238

239 A summary of test results of the undrained compression test of soils without erosion is shown in Table  
240 3. The relationships between the shear stress and the axial strain for the undrained compression tests on  
241 the soils without erosion are shown in Fig. 7 and the corresponding effective stress paths are plotted in  
242 Fig. 8. It can be seen that the uneroded soil with 35% fines content (35\_WOE\_DR30) shows the flow

243 behavior, whereas those with 15% and 25% fines contents (15\_WOE\_DR30, 25\_WOE\_DR30) shows  
244 the limited flow behavior. These indicate that the undrained mechanical behavior of the soil is  
245 influenced by the fines content and the soil becomes contractive with the increase of fines in this study.

246

247 Table 4 shows the undrained compression test results of soils with erosion, including the maximum  
248 hydraulic gradient. It can be observed that all the maximum hydraulic gradients are larger than 1.0,  
249 which is considered in the experiments to remove the majority of fines from the specimen. The  
250 hydraulic gradient of the specimen with 35% initial fines content (35\_WE\_DR30) showed the largest  
251 hydraulic gradient. It might be responsible for this mixture containing the largest amount of initial fines,  
252 which then leads to the smallest hydraulic conductivity.

253

254 Figure 9 shows the stress–strain relationships of soils with erosion. All the specimens having  
255 experienced internal erosion show a limited flow behavior. The effective stress paths of the soils with  
256 erosion are plotted in Fig. 10. It can be observed that all the eroded specimens show dilative tendency,  
257 i.e., the mean effective stress increases after passing through the phase transformation state.

258

259 The particle size analysis performed after compression tests reveal that the eroded specimens are not  
260 homogeneous, which might be responsible for the occurrence of erosion in preferential flow paths. It is  
261 considered as the inherent consequences of seepage tests.

262

### 263 **Microscopic observation**

264

265 Due to the limitation of laboratory test condition, the microscopic observation was performed at the  
266 upward seepage tests to describe the changes of particles structure induced by internal erosion. The  
267 mixtures with 15%, 25%, and 35% initial fines contents were prepared targeting a relative density of

268 30%. The moist tamping method was employed to create the similar soil fabric as that in the triaxial  
269 tests. Figure 11 shows the schematic diagram of the upward seepage test apparatus. The apparatus  
270 mainly consists of a rectangular seepage cell with a transparent glass window in front and a water  
271 reservoir. The internal dimensions of the rectangular seepage cell are 130 mm in height, 100 mm in  
272 length, and 30 mm in width. A 30 mm in thickness gravel diffusing filter was put to ensure a uniform  
273 flow across the specimens within a reasonable range. The size of the specimens is 60, 100, and 30 mm  
274 in height, length, and width, respectively.

275

276 After the preparation of specimens, a vertical stress of 50 kPa was applied to the soils to simulate the  
277 stress level in the triaxial cell under consolidation. The upward seepage flow was then applied from the  
278 bottom of the specimens after removing the vertical stress. The main objective of this test is to observe  
279 the change of soil microstructure, thus the influence of stress state is not considered at this point. The  
280 inlet flow was provided by the water reservoir, which can be raised or lowered to control its water head  
281 difference with the top of the specimens. The discharge rate was measured by the cylinder placed at the  
282 outlet from the basin. The applied maximum hydraulic gradient was large enough to dislodge most of  
283 the unstable fines away from the specimens by the assigned upward flow. In this study, the maximum  
284 applied hydraulic gradient is over 1.0.

285

286 A digital microscope with a resolution of about 1000 units  $\times$  1000 units was used to observe the  
287 distributions of fines and coarse particles during the seepage tests. The lens of the microscope was  
288 placed in front of the transparent glass window, as shown in Fig. 11.

289

290 It is well recognized that if clean sand is mixed with fines, soil microstructure will change as a  
291 consequence and that change somehow corresponds to the amount of fines content (Yamamuro and  
292 Covert 2001). An observation of the evolution of the microstructure of silica No. 3 with the increasing

293 content of silica No. 8 (i.e., 0, 15%, 25%, and 35%), regarding as fines, is presented in Fig. 12. All  
294 those moist tamped specimens have the initial relative density of 30%. Initially, without the presence of  
295 fines, the contacts between coarse particles are well developed. With the introduction of small amounts  
296 of fines (i.e., 15%), the coarse particles are coated by the fines and a fraction of fines fills the voids  
297 between coarse particles. In terms of the specimen with large amounts of fines (i.e., 25%), the dominant  
298 contact network of coarse particles might be partially destroyed, leading to more occurrence of  
299 separation of coarse particles by fine fractions. When it comes to a larger fines content (i.e., 35%), the  
300 voids between coarse particles are almost occupied by fines.

301

302 Skempton and Brogan (1994) postulated that the fines having filled the voids do not take part in the  
303 load transfer, therefore, it is expected they would be easily dislodged by the upward seepage flow. The  
304 images collected upon the completion of internal erosion (Fig. 13) proved this postulation. It is  
305 indicated that most of the fines occupying the voids formed by coarse particles were moved away by  
306 fluid flow. Although the results of upward seepage tests cannot be quantitatively compared to the  
307 downward seepage tests, they could be qualitatively correlated. For instance, fines were eroded away  
308 from specimens; hydraulic gradient and hydraulic conductivity changed; void ratios and volume of  
309 specimens were altered with the progress of internal erosion. Interestingly, at some spots, due to the  
310 small constriction size of voids, amounts of fines were impeded and consequently accumulated around  
311 the contact points of coarse particles, forming the jamming fines. Those fines would actively participate  
312 in the load transfer. Microscopically, these jammed fines may be involved in the load transfer and  
313 macroscopically they would result in different undrained responses from the soils without erosion,  
314 which will be discussed in detail later.

315

316 Albeit different, the flow direction is compared to triaxial seepage tests, the inherent mechanism of  
317 internal erosion being the same, i.e., process of fines transport. It is also argued that the fabric observed

318 through the transparent window could be different from the inside of the specimen, which might be  
319 considered as an inherent limitation for the upward seepage tests. Although the images recorded in the  
320 front of the transparent window might exaggerate the phenomenon of internal erosion, the evolutions of  
321 soil microstructure could also be presented, which is the very purpose of the upward seepage tests.  
322 Therefore, the images recorded from these tests are utilized as supplemental evidences in discussing  
323 soil mechanical behaviors in triaxial tests.

324

## 325 **Discussions**

326

327 Detailed examination of the undrained mechanical behavior can help to get a throughout understanding  
328 of the influence of fabric on soil behavior. The undrained characteristics of soil behavior at the  
329 undrained peak state, quasi-steady state, phase transformation state, and critical state are discussed in  
330 order, followed by an interpretation based on the soil fabric. The relations between the key states are  
331 presented as well.

332

### 333 **Undrained Peak State**

334

#### 335 ***Undrained peak strength***

336 The undrained peak state is the state where the shear stress reaches the initial peak in the stress–strain  
337 curve in the undrained monotonic compression test. It is associated with the onset of the flow failure  
338 (Yoshimine and Ishihara 1998). One of the soil strength parameters related to the undrained peak state  
339 is the undrained peak strength ( $s_p$ ) (Ishihara 1993), which is customarily defined as

340 (1) 
$$s_p = \frac{q_{ups}}{2}$$

341 where  $q_{ups}$  is the shear stress at the undrained peak state. Figure 14 shows the relationship between the

342 undrained peak strength normalized by initial mean effective stress and the fines content before  
343 compression. It is found that the uneroded soil with 15% initial fines content (15\_WOE\_DR30) shows  
344 larger normalized peak strength than those with 25% and 35% initial fines contents (25\_WOE\_DR30,  
345 35\_WOE\_DR30). Besides, it can be observed that the eroded soils show the larger peak strength than  
346 those of the uneroded soils with the same initial fines contents although the void ratio of the eroded  
347 soils becomes larger due to the internal erosion. Take the soils with 15% initial fines content for  
348 example, the uneroded specimen (15\_WOE\_DR30) shows normalized peak strength of 0.63, whereas  
349 the eroded specimen (15\_WE\_DR30) shows normalized peak strength of 0.85. Moreover, it can be  
350 found that the normalized peak strength of the soils with erosion is not located in the same band  
351 compared with the soils without erosion. The normalized peak strength of soils with erosion seems to  
352 be sensitive to the fines content before compression. The normalized peak strength of the soils with  
353 erosion shows different values from 0.28 to 0.85, although they contain similar fines contents around  
354 10% (ranging between 9% and 13%).

355

### 356 *Mean effective stress ratio*

357 Another important parameter at the undrained peak state is the mean effective stress ratio, which is  
358 defined as the value of mean effective stress at undrained peak state ( $p'_{ups}$ ) divided by initial mean  
359 effective stress ( $p'_o$ ) (Ishihara 1993). Figure 15 shows the mean effective stress ratio at the undrained  
360 peak state against fines content before compression.

361

362 Information about the reference data is shown in Table 5. These data are taken from the previous works  
363 on loose sands mixed with fines, prepared by the moist tamping method. It can be observed that the  
364 mean effective stress ratio is greatly influenced by the properties of tests materials. The reference data,  
365 soils with 35% initial fines content (35\_WOE\_DR30, 35\_WE\_DR30), and uneroded soil with 25%  
366 initial fines content (25\_WOE\_DR30) are located in the same band (i.e., the mean effective stress ratio

367 in between 0.5 and 0.7, irrespective to the fines content before compression). However, the mean  
368 effective stress ratios of the soils with 15% initial fines content (15\_WOE\_DR30, 15\_WE\_DR30) and  
369 the eroded soils with 25% initial fines contents (25\_WE\_DR30\_N1, 25\_WE\_DR30\_N2) are located  
370 well above the band. Although the marked difference cannot be seen in the case of the eroded soil with  
371 35% initial fines content, the mean effective stress ratios of soils with erosion are relatively larger than  
372 the soils without erosion.

373

#### 374 ***Undrained secant stiffness***

375 It is generally accepted that soil behaves nonlinearly even at a relative small strain level. Undrained  
376 secant stiffness at an axial strain in the range of 0.1%–1% is very useful in interpreting the soil  
377 behavior at initial shearing stage. Figure 16a shows the undrained secant stiffness of soils without  
378 erosion. The undrained secant stiffness here is normalized with initial mean effective stress and is  
379 plotted against the axial strain. The similar plots for the eroded soils are shown in Fig. 16b. It should be  
380 noted that the uneroded soil with 15% initial fines content (15\_WOE\_DR30) shows larger normalized  
381 secant stiffness than those with 25% and 35% initial fines contents (25\_WOE\_DR30, 35\_WOE\_DR30)  
382 when the axial strain is less than 0.9%. That is to say, the soil with smaller initial fines content indicates  
383 the larger shear stiffness than those with larger initial fines content at a small strain level. From Fig.  
384 16b, it can be observed that for the specimens with the same initial fines content, the post-erosion soil  
385 exhibits larger normalized secant stiffness compared to that without erosion when its axial strain is less  
386 than 0.4%. Take the specimens with 15% initial fines content at 0.25% axial strain for instance, the  
387 uneroded soil shows a normalized secant stiffness of 200, whereas the eroded soil shows a normalized  
388 secant stiffness of 230.

389

#### 390 **Quasi-steady state**

391

392 Another key state of the undrained behavior is the quasi-steady state where the shear stress shows a  
 393 local minimum value in the stress–strain curve. The quasi-steady state appears only when the  
 394 metastable specimens exhibit the strain softening behavior during the undrained compression. The soil  
 395 shows a minimum shear stress at the quasi-steady state, which can be even smaller than that at critical  
 396 state where the soil is sheared to a relatively larger strain. Residual strength, which is associated with  
 397 the shear stress at quasi-steady state, is recommended to use in stability analyses by Sladen et al.  
 398 (1985). They reported that the application of residual strength could be considered valid when the soil  
 399 strength is believed to be affected by some factors. Thus, it would be safer if the residual strength is  
 400 taken into consideration in analyzing the soil experienced with internal erosion.

401  
 402 The residual strength ( $s_{us}$ ) at the quasi-steady state is customarily defined as

$$403 \quad (2) \quad s_{us} = \frac{q_{qss}}{2} \cos \phi_s = \frac{M_{qss}}{2} \cos \phi_s (p'_{qss})$$

$$404 \quad (3) \quad M_{qss} = \frac{6 \sin \phi_s}{3 - \sin \phi_s}$$

405 where  $q_{qss}$  is the shear stress at the quasi-steady state,  $\phi_s$  is angle of shearing resistance at quasi-steady  
 406 state,  $p'_{qss}$  is the mean effective stress at the quasi-steady state, and  $M_{qss}$  is the shear stress ratio at the  
 407 quasi-steady state ( $q_{qss}/p'_{qss}$ ). It can be observed from Figs. 7 and 9 that all of the mixed sands with  
 408 initial fines contents of 15%, 25%, and 35% show strain softening behavior after the initial peak in the  
 409 stress–strain curves. Therefore, it can be said that the quasi-steady state appears for these specimens in  
 410 this study.

411  
 412 Figure 17 shows the shear stress ratios at the quasi-steady state against fines content before  
 413 compression on the soils with and without erosion. It is noted that the stress ratios of soils without  
 414 erosion almost stay in a narrow band of 1.30, corresponding to an angle of shearing resistance of 32.2°

415 at the quasi-steady state, irrespective of the fines content before compression. However, the shear stress  
416 ratio of soils with erosion is not a constant value and fluctuates around 1.30. This deviation from the  
417 band may suggest that the shear stress ratio at quasi-steady state also be influenced by the internal  
418 erosion.

419

420 The normalized residual strength with initial mean effective stress against fines content before  
421 compression is shown in Fig. 18. The normalized residual strengths of mixed Hokksund sand and  
422 Chengbei silt from Yang et al. (2006b) are also plotted in this figure. These mixed soils were prepared  
423 by moist tamping method with fines contents of 0, 5%, 10%, 15%, 20%, 30%, and 50%, targeting a  
424 relative density ranging from 22% to 30%. It can be observed from Fig. 18 that the normalized residual  
425 strength is affected by fines content. For the silica sand in this study, the specimens with larger fines  
426 content before compression show a smaller normalized residual strength. The normalized residual  
427 strength change with the fines content before compression in this study shows the similar tendency as  
428 the mixtures of Hokksund sand and Chengbei silt (Yang et al. 2006b).

429

430 Meanwhile, the soils with erosion show a larger normalized residual strength than the soils without  
431 erosion at the same initial fines content as for the normalized peak strength in this study. For example,  
432 at the same initial fines content of 15%, the soil without erosion shows a normalized residual strength  
433 of 0.41, but the soil with erosion shows a normalized residual strength of 0.63. This fact suggests that  
434 the soils become less contractive when they experience internal erosion.

435

### 436 **Phase transformation state**

437

438 Phase transformation state is the state where the soil shows a minimum mean effective stress in the  
439 effective stress path (Ishihara et al. 1975). It is also an indication that the soil changes from contractive

440 behavior to dilative behavior. In many cases the phase transformation state is coincident with the quasi-  
441 steady state although the definitions of these two states is different, i.e., the former is defined by the  
442 minimum mean effective stress and the latter is defined by the minimum shear stress. Typically, the  
443 quasi-steady state precedes the phase transformation state in the monotonic undrained compression.

444

445 The phase transformation state is one of the key states associated with the potential of flow failure  
446 because the value of excess pore-water pressure during compression is the maximum in this state. The  
447 flow potential ( $u_f$ ) proposed by Yoshimine and Ishihara (1998) represents the maximum excess pore-  
448 water pressure ratio during the undrained monotonic compression test, and is expressed as

449 (4) 
$$u_f = \left(1 - \frac{p'_{pts}}{p'_0}\right) \times 100\%$$

450 where  $p'_{pts}$  is the mean effective stress at the phase transformation state, and  $p'_0$  is the initial mean  
451 effective stress. The value of flow potential varies from 0 to 100%. The soil with a small value of  $u_f$   
452 means that it generates a small amount of excess pore-water pressure under the undrained compression.

453

454 The relationship between flow potential ( $u_f$ ) and fines content before compression is shown in Fig. 19.  
455 Information about the reference data is shown in Table 5. It can be seen that the uneroded soils with  
456 15%, 25%, and 35% fines contents indicate a flow potential ( $u_f$ ) ranging from 33% to 92% in this study.  
457 The flow potential is very sensitive to the fines content in the undrained compression test. In this study,  
458 the silica sand with a larger fines content before compression shows a larger flow potential than that  
459 with less fines content. The Nerlerk sand (Sladen et al. 1985) and Ottawa sand (Murthy et al. 2007)  
460 shown in Fig. 19 indicated the same tendency. That is to say, the potential of flow failure is considered  
461 higher for the soil containing a larger amount of fines.

462

463 One of the other observations from Fig. 19 is that the flow potential ( $u_f$ ) of soils with erosion is smaller

464 than that of soils without erosion at the same initial fines content. Taking the soils with 15% initial  
465 fines content for example, the flow potential ( $u_f$ ) of soil without erosion (15\_WOE\_DR30) is 33%,  
466 whereas that of soil with erosion (15\_WE\_DR30) decreases to 0.5%. In addition, the slopes of the  
467 relationship between the fines content before compression and flow potential are more or less the same  
468 for the soils without erosion as indicated in the dash lines, while it is steeper for the eroded soil (dotted  
469 line in Fig. 19). This difference indicates that the compressibility of the eroded soil is more sensitive to  
470 the fines content compared to the uneroded soils.

471

### 472 **Critical state**

473

474 The concept of critical state is an effective and useful framework for discussing the soil behavior,  
475 which is defined as the state where the soils continue to deform without change of effective stress or  
476 migration of pore water (Roscoe et al. 1958). The pioneer study on the evolution of CSL with erosion  
477 is presented by Muir Wood (2007) by adopting the concept of “grading state index”. In their approach,  
478 “grading state index” is defined as the ratio of the current grading to the limiting grading, which varies  
479 from 0 to 1 corresponding to the changes from single sized grading to certain limiting grading. The  
480 direct consequences of internal erosion include the movement of particle grading curve due to the  
481 amounts of fines loss, which accordingly changes the grading state index. Figure 20 indicates the  
482 movement of particle grading curves of the tested specimens (25\_WOE\_DR30, 25\_WE\_DR30\_N2)  
483 induced by internal erosion. Coincident with the studies of Muir Wood and Maeda (2008) and Muir  
484 Wood et al. (2010), the grading curve moves downward after internal erosion and the extent of that  
485 movement may represent the amounts of fines loss, suggesting a decline in grading state index. Further,  
486 it may cause the upward movement of CSL in the  $e$ - $\log p'$  plane.

487

488 In this study, the undrained test data were interpreted to understand the corresponding evolution of

489 CSL with internal erosion. For those cases without sufficient straining, a sigmoidal function fitting  
490 proposed by Murthy et al. (2007) was utilized to extrapolate the critical state, the details of which are  
491 explained in Appendix A. Figure 21 shows the critical state of soils before and after erosion. The CSL  
492 of the uneroded specimens with 35% fines content was derived from the results of the laboratory  
493 compression tests. Unfortunately, similar tests on the specimens with 15% and 25% fines contents have  
494 not been performed. Therefore, the CSLs of soils with 15% and 25% fines contents, shown in Fig. 21,  
495 were postulated on the basis that the soil with a smaller fines content shows a steeper CSL in the  $e$ - $\log$   
496  $p'$  plane (Murthy et al. 2007). Zlativoc and Ishihara (1997) concluded that critical state may erase the  
497 influence of initial fabric and in this circumstance the soil mechanical responses tend to become similar.  
498 It is noted from Table 4 that the fines contents of eroded specimens before compression are similar,  
499 ranging from 9% to 13%. Therefore, it can be assumed that the critical states of the eroded specimens  
500 somehow locate on a similar CSL, which is above that of the uneroded specimens. The movement of  
501 CSL is in accordance with the theoretical prediction of Muir Wood and Maeda (2008) and Muir Wood  
502 et al. (2010): due to the decrease of grading state index induced by internal erosion the CSL in the  $e$ - $\log$   
503  $p'$  plane moves upwardly.

504

#### 505 **Effects of fines content on undrained behavior**

506

507 As shown in the previous subsections, the uneroded specimens containing a smaller amount of fines  
508 show a larger value of peak strength, undrained secant stiffness, and residual strength than that  
509 containing a larger amount of fines. These undrained behaviors on the soils without erosion may be  
510 affected by the soil fabric.

511

512 All the specimens in this study were prepared by moist tamping method. It is well known that the moist  
513 tamping method would create metastable honeycomb structures among coarse particles. The images in

514 Fig. 12 taken by a digital microscope reveal the micro soil fabric to some extent in this study. The  
515 honeycomb structure can be clearly observed in the soil with 15% fines content because the voids  
516 between coarse particles are hardly filled with fines. However, in the soil with 25% fines content, the  
517 voids between coarse particles are partially filled with fines. In the soil with 35% fines content, these  
518 voids are largely filled with fines. Most of the coarse grains seem to be floating on the fines. Therefore,  
519 the honeycomb structure cannot be obviously observed in the soils with 25% and 35% fines contents.

520

521 Observations of the contacts in the binary soil mixtures are formed randomly by fines and coarse  
522 particles. The fines in between the coarse particles in the soil with 15% fines content are less than those  
523 in the soils with 25% and 35% fines contents. It might be possible to assume that the amount of the  
524 jamming fines is less in the soil with 15% fines content. According to Salgado et al. (2000), during  
525 compression, the coarse particles may be easily moved side away for the soil with less jamming fines  
526 (i.e., soil with 15% fines content), leading to greater direct contacts between coarse particles during  
527 shearing. The load may be more efficiently transferred through the coarse particles than through the  
528 fines. Therefore, it is possible to deduce that the uneroded soil with smaller fines content would show a  
529 relatively larger peak and residual strength than that with larger fines content within the test range.

530

### 531 **Summary of effects of internal erosion on undrained behavior**

532

533 Through the comparison between the soils with and without erosion, it is noted that the undrained  
534 behavior of the eroded soils is different from that of the uneroded soils. The soils with erosion show a  
535 larger peak and residual strength than those without erosion, which probably means that the soils  
536 become less contractive after internal erosion. One of the reasons for the dilative behavior of soils with  
537 erosion might be the dilative characteristic of silica No. 3. As indicated in Figs. 7 and 8, the specimens  
538 made of silica No. 3 only show a fully dilative behavior in the undrained compression test even at loose

539 condition (initial relative density of 20% and 30%).

540

541 The soils with erosion have similar fines content before compression, but they showed different  
542 behavior during the undrained compression tests. For instance, the flow potential of eroded soils shows  
543 a wide range of value within only a small range of fines content. Therefore, it could be said that the  
544 reason of the difference in the undrained behavior of soils with and without erosion is caused not only  
545 by the decrease of fines content because of internal erosion, but also by the change of the fabric. In this  
546 study, the soil fabric is observed by digital microscope and the collected images of soils subjected to  
547 internal erosion can be seen in Fig. 13.

548

549 The coarse particles of the soils with erosion were rearranged due to the internal erosion. The  
550 transportation of fines leads to an increase of void space. The hydraulic force induced by the seepage  
551 flow not only transports the fines, but also changes the position of the coarse particles, which may have  
552 resulted in a fabric that is different from the soils without erosion. This probably changes the way of  
553 load transferring in the soils with erosion compared with the soils without erosion.

554

555 The contacts between particles may also have been changed by the internal erosion. It can be observed  
556 in Fig. 13 that some fines still stay in between the coarse particles after the seepage test. During the  
557 progress of the seepage flow, the fines were jammed in the slaps around the contact points between the  
558 coarse particles. Thus, the number of the effective contact points increases due to the internal erosion,  
559 resulting in a much more efficient transformation of the internal forces.

560

### 561 **Relation between key states**

562

563 The soils used in this study show a local maximum shear stress at the undrained peak state and a

564 minimum shear stress at the quasi-steady state. The local minimum mean effective stress appears at the  
565 phase transformation state. The relationships between these states are compared below.

566

### 567 ***Undrained peak state and quasi-steady state***

568 The tested specimens mostly exhibit initial peak strength followed by a local minimum in the stress–  
569 strain curve, which corresponds to the residual strength at the quasi-steady state. The relationship of the  
570 shear stress normalized by the initial mean effective stress between the undrained peak state and quasi-  
571 steady state is shown in Fig. 22. According to the definition of the undrained peak state and quasi-  
572 steady state, the shear stress at the former state would always be larger or equal to that at the latter state.  
573 To show the relationship clearly, a demarcation line where the shear stress at undrained peak state  
574 equals to that at quasi-steady state is also drawn as the solid line in Fig. 22. If the difference between  
575 the normalized peak strength and normalized residual strength is small, the state point is located around  
576 the demarcation line, suggesting a less contractive behavior. For example, the specimens  
577 25\_WOE\_DR30\_N1 and 25\_WE\_DR30\_N2 show a relatively less contractive behavior, so their states  
578 locate very near the demarcation line. It can be noted that, by comparing the relative position of the  
579 points to the demarcation line, the points for the eroded soils are closer to the demarcation line,  
580 suggesting a less contractive response.

581

### 582 ***Undrained peak state and phase transformation state***

583 The undrained peak state is associated with the onset of flow failure, and the phase transformation state  
584 is the state where soil behavior changes from contractive to dilative. Between these two states, a  
585 relatively small load might be sufficient to cause a large deformation of soil structure. That is to say,  
586 the soil would experience an instability state between the undrained peaks state and phase  
587 transformation state (Leong and Chu 2002).

588

589 The instability line is defined as the line connecting points of the shear stress at the undrained peak  
590 state in the effective stress plane. Yang et al. (2006a) found that the instability line passes through the  
591 origin in the effective stress plane for the cohesionless soils. Therefore, the instability line here is  
592 described as the line connecting the origin to the point at the undrained peak state in the effective stress  
593 path. The instability zone is defined as the zone between the instability line and the line connecting the  
594 origin to the phase transformation state in the effective stress plane.

595

596 The normalized slope differences against the fines content before compression are shown in Fig. 23.  
597 The normalized slope difference here is defined as the difference between the slope of the line  
598 connecting the origin to the phase transformation state and that of the instability line in the effective  
599 stress plane, normalized by the slope of the line connecting the origin to the phase transformation state.  
600 It enables to quantitatively evaluate the instability zone: the soil with a larger slope difference indicates  
601 a wider instability zone. It is noted that the slope differences of soils with erosion are larger than those  
602 of soils without erosion at the same initial fines content, especially for the soil with 25% initial fines  
603 content, the slope difference of that without erosion (25\_WOE\_DR30) is 0.28, whereas the average  
604 slope difference of that with erosion (25\_WE\_DR30\_N1, 25\_WE\_DR30\_N2) is 0.48, suggesting that  
605 the instability zone is enlarged by the internal erosion. The big change in the slope difference between  
606 the eroded soils and uneroded soils might have resulted from the drastic change of its fabric due to  
607 internal erosion. Intergranular void ratio assumes that fines function as voids and therefore the volume  
608 of fines is considered as voids. Accordingly, if the intergranular void ratios of soils before and after  
609 seepage tests are similar, the specimen losing larger volume of fines would have greater deformation to  
610 compensate the changes in volumes of voids, which might indicate greater changes of fabric. Table 2  
611 notes that the intergranular void ratios of specimens with 15% and 25% initial fines contents are similar  
612 before and after erosion, but more fines are eroded away from the specimen with 25% initial fines  
613 content. Therefore, the fabric change of specimen with 25% initial fines content should be greater than

614 that of specimen with 15% initial fines content. This tendency corresponds to a larger change of slope  
615 difference for specimen with 25% initial fines content (Fig. 23). In contrast, the intergranular void ratio  
616 of the specimen with 35% initial fines content decreases after erosion, which suggests that the coarse  
617 fraction is further compacted after internal erosion. Although the specimen with 35% initial fines  
618 content shows the largest cumulative eroded soil mass, the balance between the amounts of fines  
619 erosion and compaction of coarse fraction leads to less change of its slope difference than that of  
620 specimen with 25% initial fines content. Future study on the fabric of soils subjected to internal erosion  
621 might be helpful in understanding its mechanic consequences.

622

## 623 **Conclusions**

624

625 Seepage tests and undrained monotonic compression tests were performed to examine the influence of  
626 initial fines content on (i) the seepage-induced fabric change and (ii) mechanical consequences of soils  
627 subjected to internal erosion. The images of the packing of the soil particles were taken by a digital  
628 microscope to observe the fabric change before and after the internal erosion. It is found that the  
629 seepage flow not only transports fines away from the specimen, but causes a drastic change in the soil  
630 fabric, which results in a totally different undrained mechanical behavior for soils with erosion  
631 compared with those without erosion. During the seepage tests, the soil with larger initial fines content  
632 shows a larger amount of cumulative eroded soil mass and a larger volumetric strain within the test  
633 range.

634

635 The images collected before and after internal erosion reveal that the soil fabric is altered by the  
636 internal erosion. In the uneroded soil with fines, the coarse particles are coated by fines and the  
637 distribution of the fines varies with the fines content. While for the soils with erosion, most of  
638 remaining fines are jammed around the contact between coarse particles, which results in an increase of

639 the number of effective contact points.

640

641 The amounts of silica No. 8 in the tested mixtures would greatly affect their undrained behavior,  
642 resulting in the changes of peak strength and residual strength. Specifically, a smaller content of silica  
643 No. 8 would cause a larger peak, residual strength, and correspondingly a smaller flow potential.

644

645 The internal erosion may change the soil fabric and further influences the undrained behavior. The  
646 mean effective stress ratios (ratio of mean effective stress at peak to that at initial) of soil with erosion  
647 show different values from the soil without erosion. For the specimens with the same initial fines  
648 content, the post-erosion soil exhibits larger undrained secant stiffness compared to that without  
649 erosion at a relatively small axial strain level. The soils with erosion show larger residual strength than  
650 those without erosion if their initial fines contents are the same. Meanwhile, the eroded soils generate a  
651 smaller amount of excess pore-water pressure than the uneroded soils before reaching the phase  
652 transformation state. It is also noted that the slope difference between the line connecting the origin to  
653 the transformation state and the instability line in the effective stress plane is larger for the soils with  
654 erosion, indicating an enlarged instability zone after internal erosion.

655

## 656 **Acknowledgement**

657

658 Support for the first author is provided by a Monbukagakusho (Ministry of Education, Culture, Sports,  
659 Science and Technology, Japan) scholarship for graduate students. This work is financially supported  
660 by JSPS KAKENHI Grant No. 25420498. The authors express gratitude to their colleagues at Tokyo  
661 Institute of Technology, particularly Ke Lin, for their important contributions.

662

663 **References**

664

665 Abedi, M., and Yasrobi, S.S. 2010. Effects of plastic fines on the instability of sand. *Soil Dynamics*  
666 *and Earthquake Engineering*, 30(3): 61–67.

667 Alarcon-Guzman, A., Leonards, G., and Chameau, J. 1988. Undrained monotonic and cyclic strength  
668 of sands. *Journal of Geotechnical Engineering*, 114(10): 1089–1109.

669 ASTM D4767-11. 2012. Standard test method for consolidated undrained triaxial compression test for  
670 cohesive soils. Annual book of ASTM standards, Vol.04.08, ASTM International, West  
671 Conshohocken.

672 Bonelli, S. 2012. *Erosion of geomaterials*. Wiley.

673 Cividini, A., Bonomi, S., Vignati, G.C., and Gioda, G. 2009. Seepage-induced erosion in granular soil  
674 and consequent settlements. *International Journal of Geomechanics*, 9(4): 187–194.

675 Cividini, A., and Gioda, G. 2004. Finite-element approach to the erosion and transportation of fine  
676 particles in granular soils. *International Journal of Geomechanics*, 4(3): 191-198.

677 Ishihara, K., Tatsuoka, F., and Yasuda, S. 1975. Undrained deformation and liquefaction of sand under  
678 cyclic stresses. *Soils and Foundations*. 15(1): 29-44.

679 Ishihara, K. 1993. Liquefaction and flow failure during earthquakes. *Géotechnique*, 43(3): 351–451.

680 JGS 0525-2000. 2000. Method for  $k_0$  consolidated-undrained triaxial compression test on soils with  
681 pore water pressure measurement. Standards of Japanese Geotechnical Society for Laboratory  
682 Shear Tests, Japanese Geotechnical Society: pp. 28-34.

683 Ke, L., and Takahashi, A. 2012. Strength reduction of cohesionless soil due to internal erosion induced  
684 by one-dimensional upward seepage flow. *Soils and Foundations*, 52(4): 698–711.

685 Ke, L., and Takahashi, A. 2014a. Triaxial erosion test for evaluation of mechanical consequences of

686 internal erosion. *Geotechnical Testing Journal*, 37(2): 1–18.

687 Ke, L., and Takahashi, A. 2014b. Experimental investigations on suffusion characteristics and its  
688 mechanical consequences on saturated cohesionless soil. *Soils and Foundations*, 54(4): 713-730.

689 Kenney, T.C., and Lau, D. 1985. Internal stability of granular filters. *Canadian Geotechnical Journal*,  
690 22(2): 215–225.

691 Ladd, R.S. 1978. Preparing test specimens using undercompaction. *Geotechnical Testing Journal*, 1(1):  
692 16–23.

693 Lade, P.V., and Yamamuro, J.A. 1997. Effects of nonplastic fines on static liquefaction of sands.  
694 *Canadian Geotechnical Journal*, 34(6): 918–928.

695 Leong, W.K., and Chu, J. 2002. Effect of undrained creep on instability behavior of loose sand.  
696 *Canadian Geotechnical Journal*, 39(6): 1399–1405.

697 Mitchell, J., and Soga, K. 2005. *Fundamentals of soil behavior*. Wiley.

698 Moffat, R., and Fannin, R.J. 2011. A hydromechanical relation governing internal stability of  
699 cohesionless soil. *Canadian Geotechnical Journal*, 48(3): 413-424.

700 Moffat, R., Fannin, R.J., and Garner, S.J. 2011. Spatial and temporal progression of internal erosion in  
701 cohesionless soil. *Canadian Geotechnical Journal*, 48(3): 399-412.

702 Muir Wood, D. 1990. *Soil behaviour and critical state soil mechanics*. Cambridge University Press.

703 Muir Wood, D. 2007. The magic of sands. 20th Bjerrum Lecture, presented in Oslo 25 November 2005.  
704 *Canadian Geotechnical Journal*, 44(11): 1329-1350.

705 Muir Wood, D., Maeda, K., and Nukudani, E. 2010. Modelling mechanical consequences of erosion.  
706 *Géotechnique*, 60(6): 447–457.

707 Muir Wood, D., and Maeda, K. 2008. Changing grading of soil: effect on critical states. *Acta*

708 Geotechnica, 3(1): 3-14.

709 Murthy, T.G., Loukidis, D., Carraro, J.A.H., Prezzi, M., and Salgado, R. 2007. Undrained monotonic  
710 response of clean and silty sands. *Géotechnique*, 57(3): 273–288.

711 Ni, Q., Tan, T.S., Dasari, G.R., and Hight, D.W. 2004. Contribution of fines to the compressive  
712 strength of mixed soils. *Géotechnique*, 54(9): 561–569.

713 Rahman, M.M., Lo, S.R., and Baki, M.A.L. 2011. Equivalent granular state parameter and undrained  
714 behaviour of sandfines mixtures. *Acta Geotechnica*, 6(4): 183–194.

715 Rao, S.S. 2009. *Engineering optimization: theory and practice*. John Wiley & Sons.

716 Roscoe, K.H., Schofield, A.N., and Wroth, C.P. 1958. On the yielding of soils. *Géotechnique*, 8(1): 22-  
717 52.

718 Salgado, R., Bandini, P., and Karim, A. 2000. Shear strength and stiffness of silty sand. *Journal of*  
719 *Geotechnical and Geoenvironmental Engineering*, 126(5):451–462.

720 Scholtés, L., Hicher, P.Y., and Sibille, L. 2010. Multiscale approaches to describe mechanical  
721 responses induced by particle removal in granular materials. *Comptes Rendus Mécanique*, 338(10-  
722 11): 627–638.

723 Skempton, A.W., and Brogan, J.M. 1994. Experiments on piping in sandy gravels. *Géotechnique*, 44(3):  
724 449-460.

725 Sladen, J.A., D'Hollander, R.D., and Krahn, J. 1985. The liquefaction of sands, a collapse surface  
726 approach. *Canadian Geotechnical Journal*, 22(4): 564–578.

727 Sterpi, D. 2003. Effects of the erosion and transportation of fine particles due to seepage flow.  
728 *International Journal of Geomechanics*, 3(1): 111-122.

729 Thevanayagam, S. 1998. Effect of fines and confining stress on undrained shear strength of silty sands.  
730 *Journal of Geotechnical and Geoenvironmental Engineering*, 124(6): 479–491.

- 731 Thevanayagam, S., and Mohan, S. 2000. Intergranular state variables and stress-strain behaviour of  
732 silty sands. *Géotechnique*, 50(1): 1–23.
- 733 Tsukamoto, Y., Ishihara, K., and Kamata, T. 2009. Undrained shear strength of soils under flow  
734 deformation. *Géotechnique*, 59(5): 483–486.
- 735 U.S. Department of Agriculture (USDA). 1994. Gradation design of sand and gravel filters. Chapter 26,  
736 National engineering handbook, Part 33, Soil Conservation Service, Washington, D.C.
- 737 Vaid, Y.P., Chung, E.K.F., and Kuerbis, R.H. 1990. Stress path and steady state. *Canadian*  
738 *Geotechnical Journal*, 21(1): 1–7.
- 739 Yamamuro, J., and Covert, K. 2001. Monotonic and cyclic liquefaction of very loose sands with high  
740 silt content. *Journal of Geotechnical and Geoenvironmental Engineering*, 127(4): 314–324.
- 741 Yang, S.L., Sandven, R., and Grande, L. 2006a. Instability of sand silt mixtures. *Soil Dynamics and*  
742 *Earthquake Engineering*, 26(2-4): 183–190.
- 743 Yang, S.L., Sandven, R., and Grande, L. 2006b. Steady-state lines of sand-silt mixtures. *Canadian*  
744 *Geotechnical Journal*, 43(11): 1213–1219.
- 745 Yang, Z.X., Li, X.S., and Yang, Y. 2008. Quantifying and modelling fabric anisotropy of granular soils.  
746 *Géotechnique*, 58(4): 237–248.
- 747 Yoshimine, M., and Ishihara, K. 1998. Flow potential of sand during liquefaction. *Soils and*  
748 *Foundations*, 38(3): 189–198.
- 749 Zlativoc, S., and Ishihara, K. 1997. Normalized behavior of very loose non-plastic soils: effects of  
750 fabric. *Soils and Foundations*, 37(4): 47-56.
- 751

752 Table 1. Properties of tested materials

	Silica No. 3	Specimen 15	Specimen 25	Specimen 35	Silica No.8
Fines content (%)	0	15.0	25.0	35.0	100
Maximum void ratio	0.94	0.79	0.77	0.74	1.33
Minimum void ratio	0.65	0.53	0.37	0.36	0.70
Median particle size (mm)	1.76	1.78	1.69	1.54	0.16
Curvature coefficient	0.96	8.69	8.54	0.074	0.99
Uniformity coefficient	1.31	13.0	16.4	19.3	1.05

753

754 Table 2. Seepage tests results

Specimen No.	$F_c^a$ (%)	$e_0^b$	$e_c^c$	$e_{cs}^d$	$F_{ce}^e$ (%)	$e_e^f$	$e_{es}^g$	$\varepsilon_v^h$ (%)
15_WE_DR30	15	0.68	0.67	0.96	8.75	0.80	0.98	0.11
25_WE_DR30_N1	25	0.61	0.56	1.08	12.0	0.81	1.06	1.62
25_WE_DR30_N2	25	0.61	0.54	1.05	13.1	0.81	1.06	2.21
35_DR30_WE	35	0.61	0.59	1.45	13.3	0.99	1.29	10.1

755 <sup>a</sup>Initial fines content,  $F_c$  (%).

756 <sup>b</sup>Initial void ratio,  $e_0$ .

757 <sup>c</sup>Void ratio after consolidation,  $e_c$ .

758 <sup>d</sup>Intergranular void ratio after consolidation (before seepage test),  $e_{cs}=(e_c+F_c/100)/(1-F_c/100)$ .

759 <sup>e</sup>Fines content after seepage test,  $F_{ce}$  (%).

760 <sup>f</sup>Void ratio after seepage test,  $e_e$ .

761 <sup>g</sup>Intergranular void ratio after seepage test,  $e_{es}=(e_e+F_{ce}/100)/(1-F_{ce}/100)$ .

762 <sup>h</sup>Volumetric strain,  $\varepsilon_v$  (%).

763

764 Table 3. Undrained compression test results of soils without erosion

Specimen No.	Fines content, $F_c$ (%)	Initial void ratio, $e_0$	Void ratio after consolidation, $e_c$	Axial strain at undrained peak state (%)	Axial stain at quasi-steady state (%)	Axial strain at phase transformation state (%)
00_WOE_DR20	0	0.84	0.84	--	--	--
00_WOE_DR30	0	0.82	0.82	--	--	--
15_WOE_DR30	15	0.68	0.67	0.99	3.92	4.58
25_WOE_DR30	25	0.61	0.56	2.27	2.34	3.60
35_WOE_DR30	35	0.60	0.56	0.58	8.11	8.59

765

766

767 Table 4. Undrained compression test results of soils with erosion

Specimen No.	Fines content after seepage test, $F_{ce}$ (%)	Void ratio after consolidation, $e_c$	Maximum hydraulic gradient, $i_{max}$	Void ratio after seepage test, $e_e$	Axial strain at undrained peak state (%)	Axial stain at quasi-steady state (%)	Axial strain at phase transformation state (%)
15_WE_DR30	8.75	0.67	2.07	0.80	1.00	3.77	4.92
25_WE_DR30 _N1	12.0	0.56	5.05	0.81	1.93	3.93	6.59
25_WE_DR30 _N2	13.1	0.54	5.39	0.81	2.20	4.64	4.70
35_WE_DR30	13.3	0.59	11.7	0.99	1.07	4.83	6.06

768

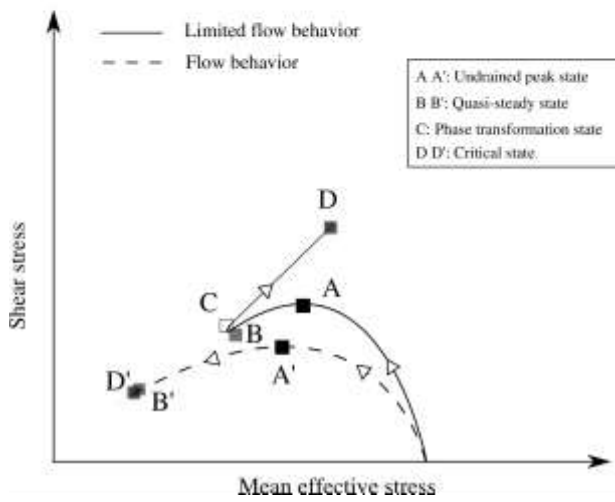
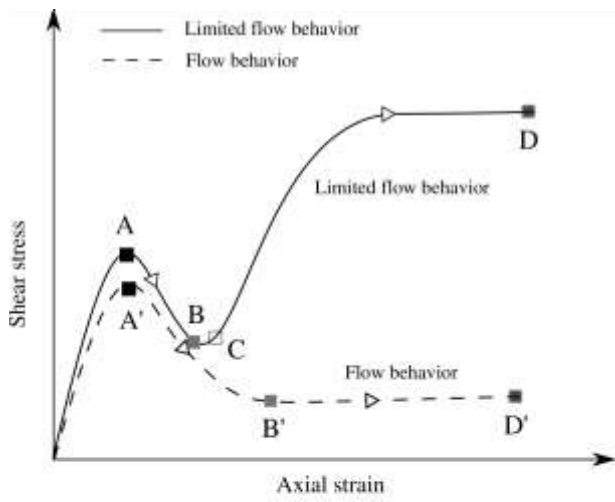
769

770 Table 5. Information of reference data

Tested materials	Fines content (%)	Relative density (%)	Preparation method	References
Leighton Buzzard sand, Nerlerk sand	0, 2.2, 12	10 - 30	Moist tamping	Sladen et al. 1985
Toyoura sand	0	7 - 65	Moist tamping	Ishihara 1993
Ottawa sand	0, 5, 10, 15	20 - 50	Moist tamping	Murthy et al. 2007

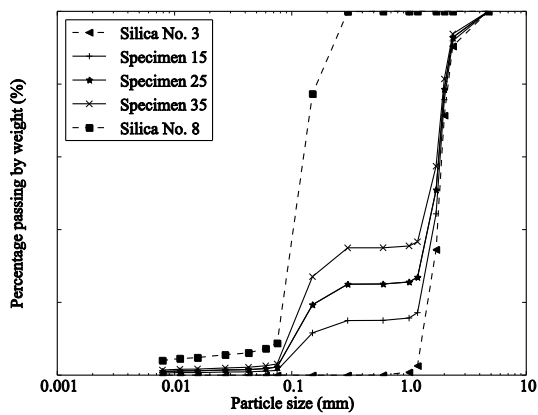
771

772



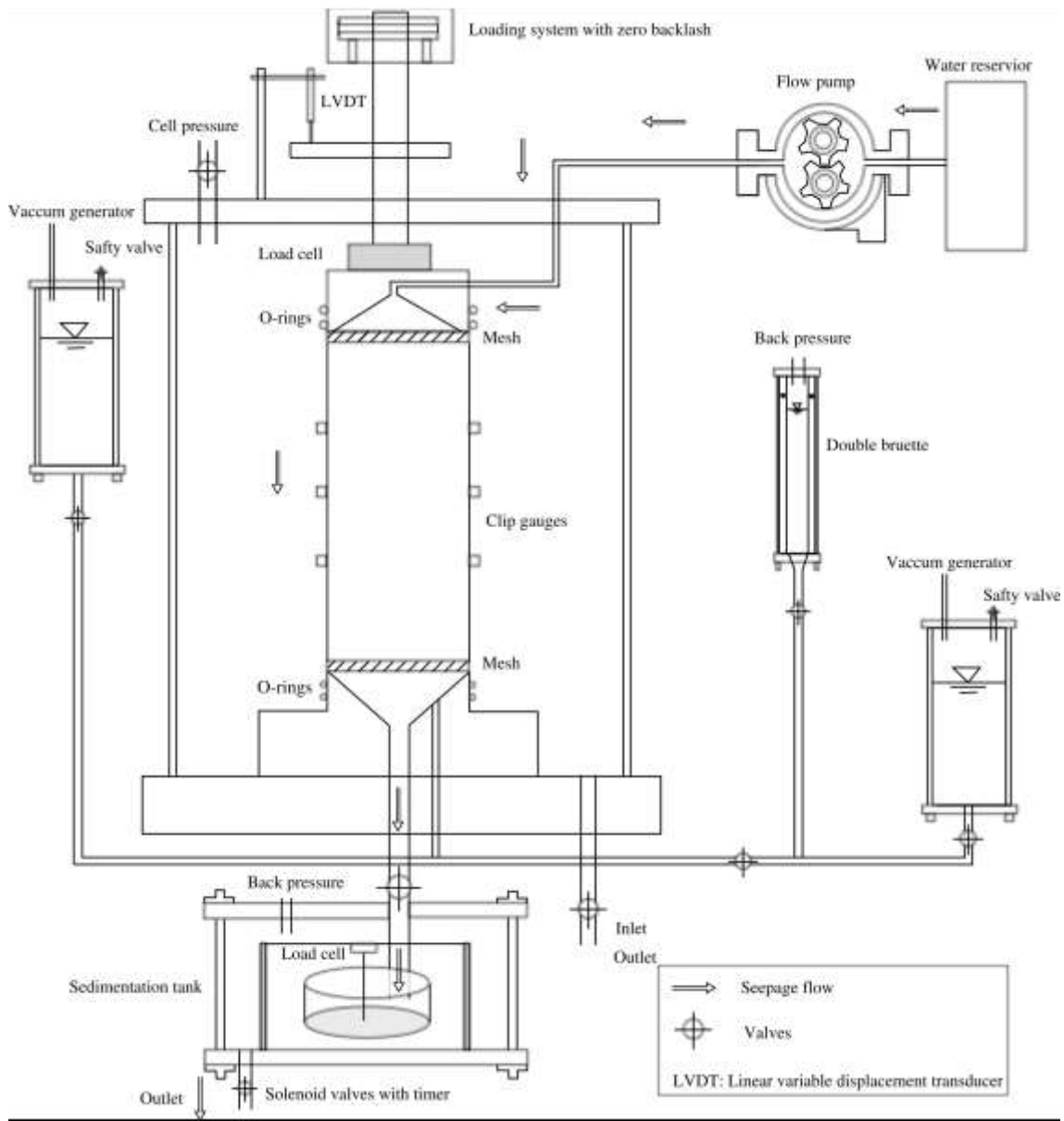
773

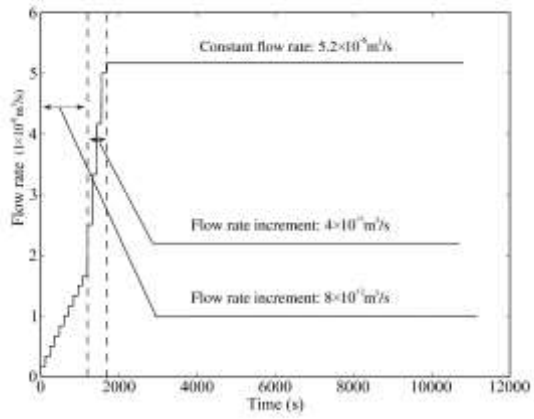
774 Fig. 1. Schematic diagram of the characteristics of typical undrained behaviors



775

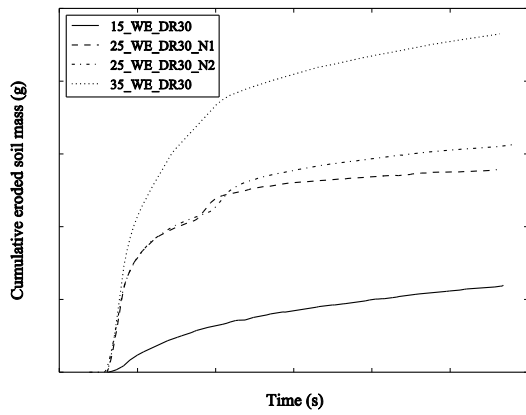
776 Fig. 2. Particle size distribution curves





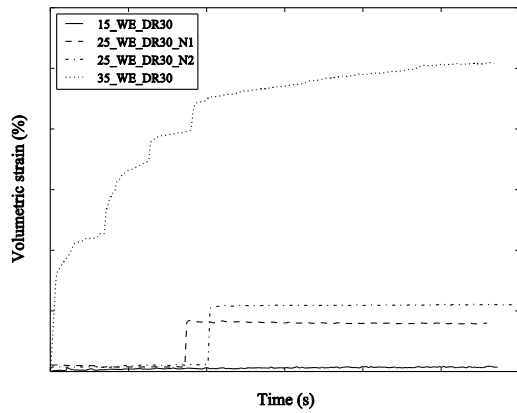
780

781 Fig. 4. Flow rate in seepage test



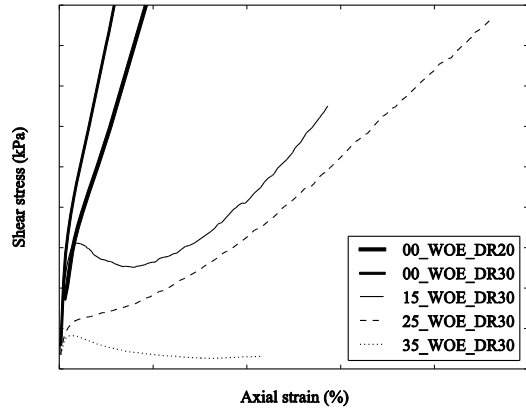
782

783 Fig. 5. Evolution of cumulative eroded soil mass during seepage test



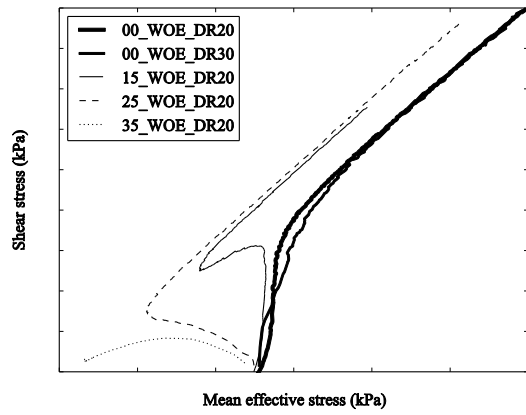
784

785 Fig. 6. Evolution of volumetric strain during seepage test



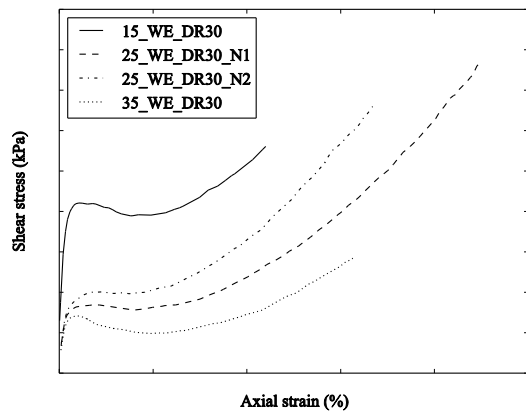
786

787 Fig. 7. Stress-strain curves of soils without erosion



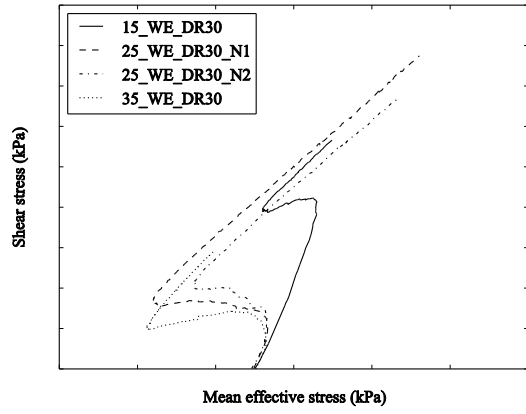
788

789 Fig. 8. Effective stress paths of soils without erosion



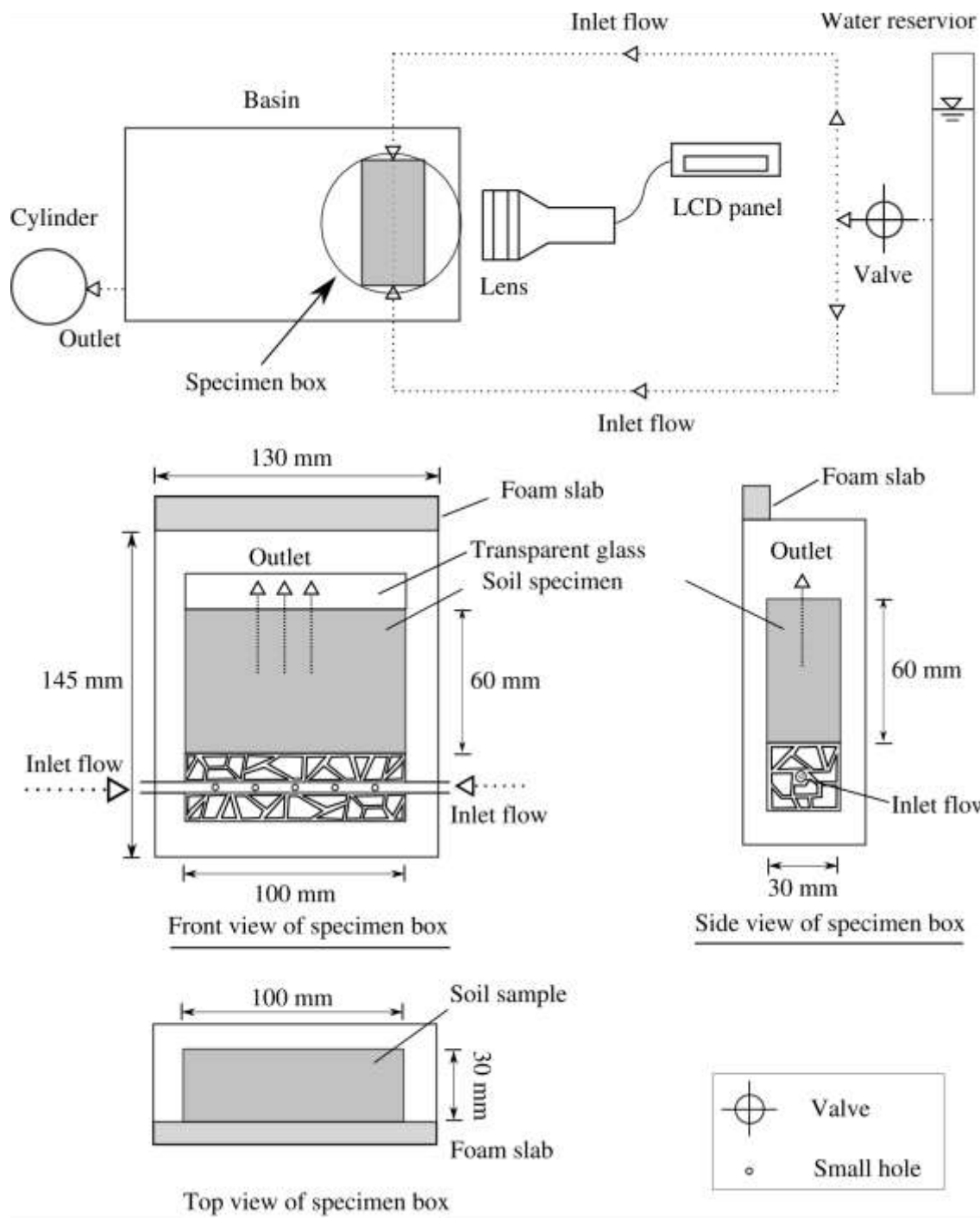
790

791 Fig. 9. Stress-strain curves of soils with erosion



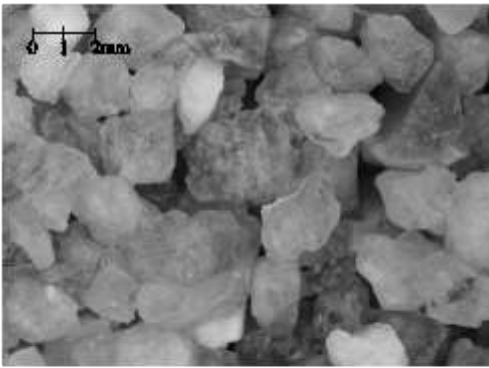
792

793 Fig. 10. Effective stress paths of soils with erosion

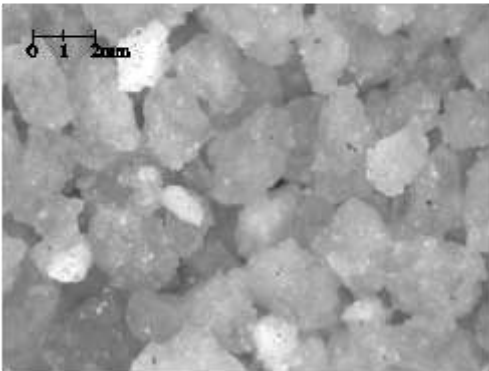


794

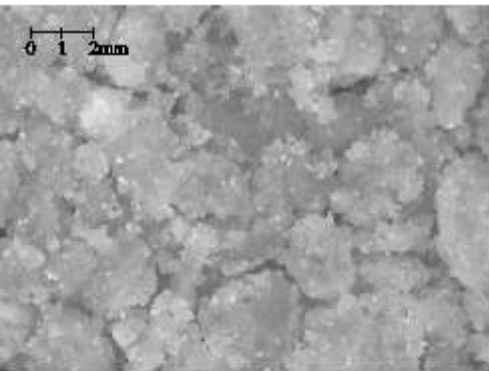
795 Fig. 11. Apparatus for upward seepage test



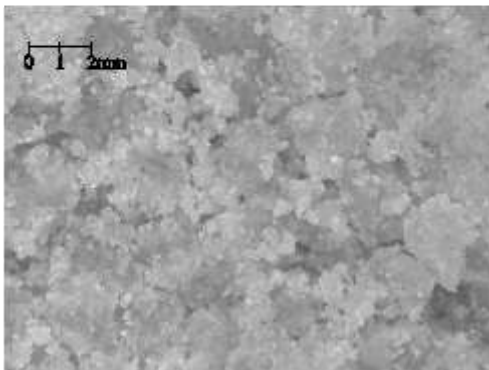
(a) Before erosion (0% initial fines content)



(b) Before erosion (15% initial fines content)



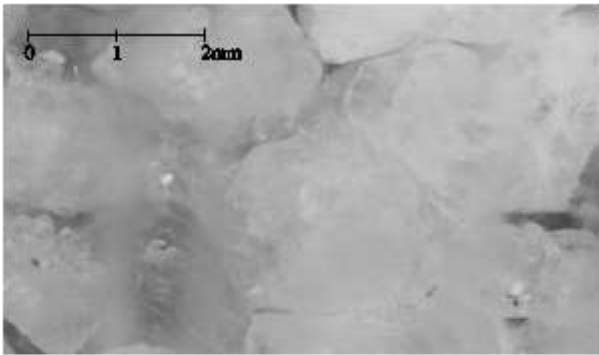
(c) Before erosion (25% initial fines content)



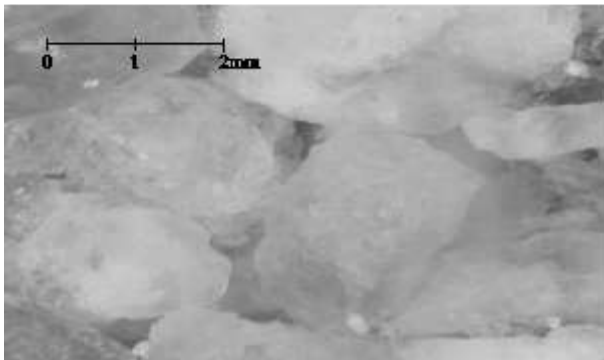
(d) Before erosion (35% initial fines content)

796

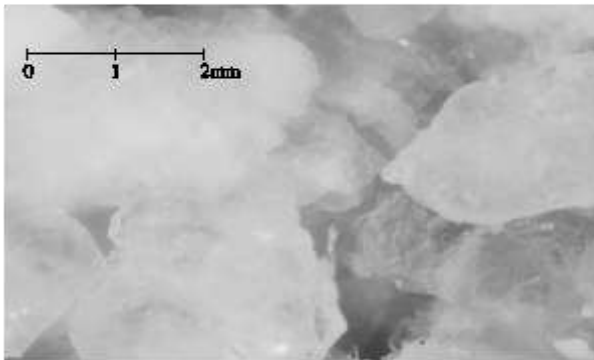
797 Fig. 12. Micro-structure of soils without erosion



(a) After erosion (15% initial fines content)



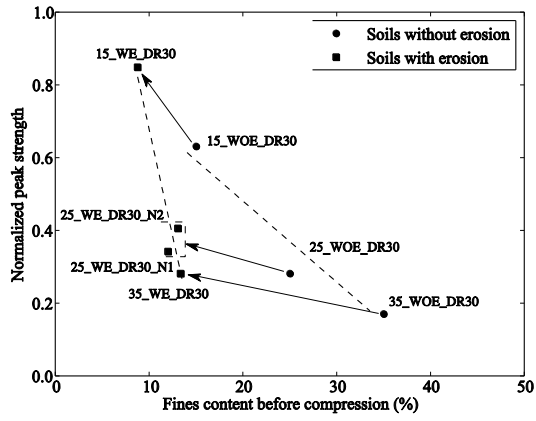
(b) After erosion (25% initial fines content)



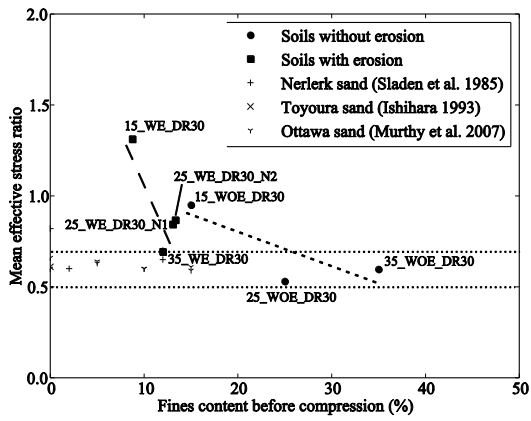
(c) After erosion (35% initial fines content)

798

799 Fig. 13. Micro-structure of soils with erosion



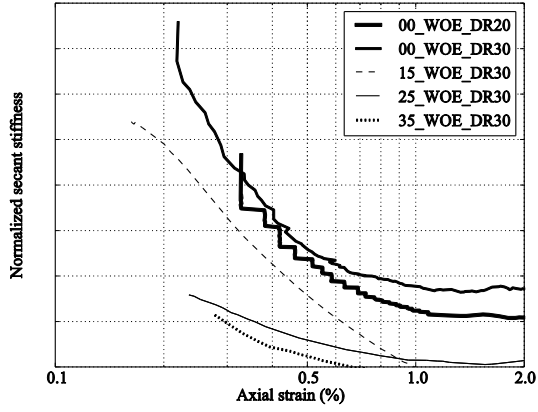
800  
801 Fig. 14. Normalized peak strength against fines content before compression



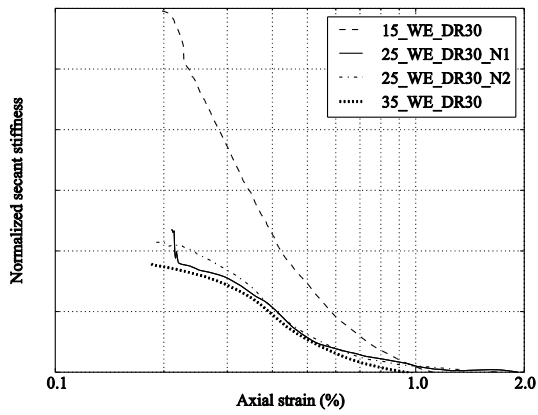
802  
803 Fig. 15. Mean effective stress ratios against fines content before compression

804

805

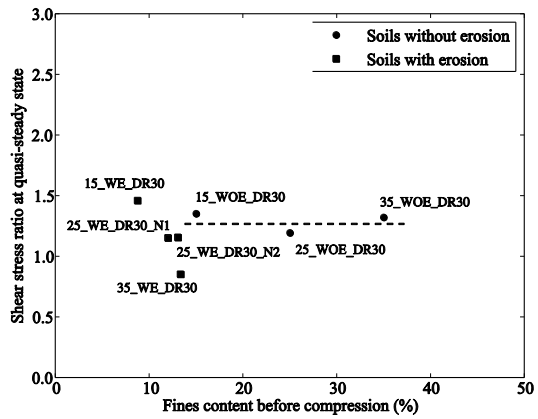


806

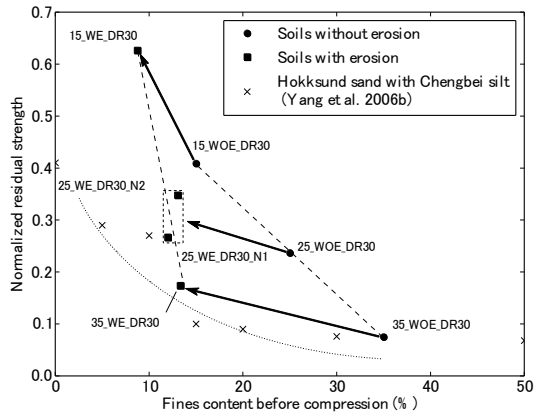


807 Fig. 16. Relation between normalized secant stiffness and axial strain

808

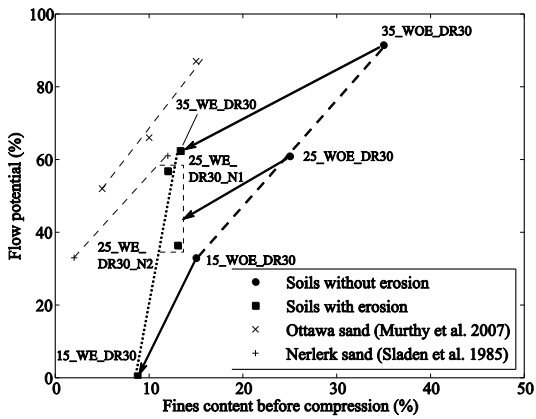


809 Fig. 17. Shear stress ratios at quasi-steady state against fines content before compression



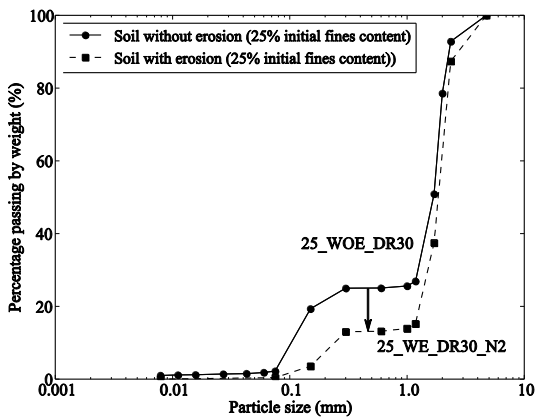
810

811 Fig. 18. Normalized residual strength against fines content before compression



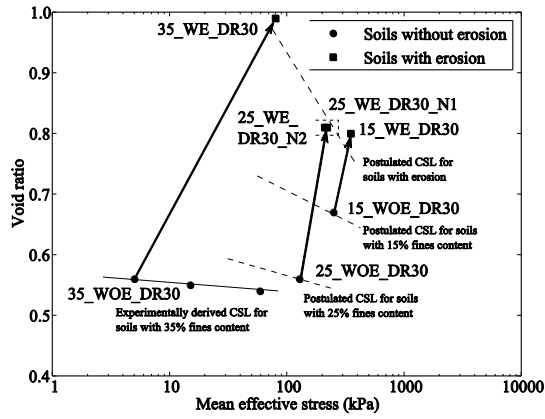
812

813 Fig. 19. Flow potential against fines content before compression



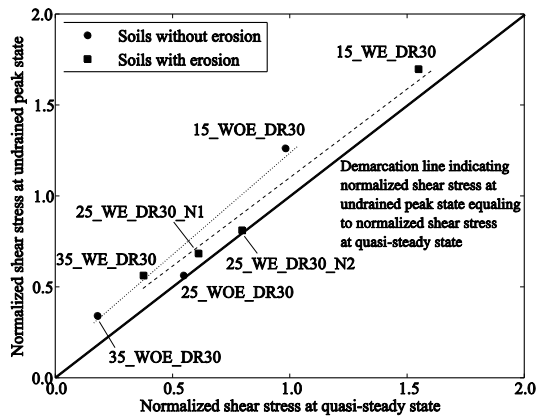
814

815 Fig. 20. Movement of particle grading curves



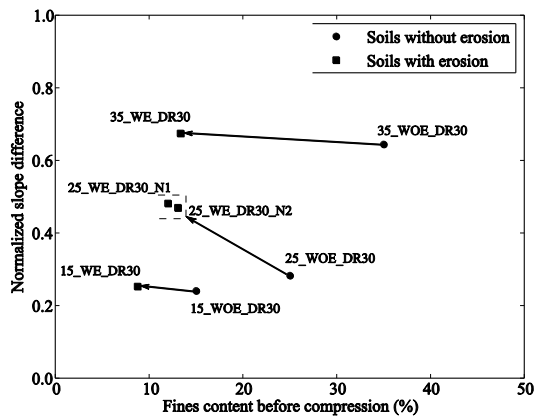
816

817 Fig. 21. Critical states of tested specimens in  $e$ - $\log p'$  plane



818

819 Fig. 22. Relation of normalized shear stress at undrained peak state and quasi-steady state



820

821 Fig. 23. Slope difference against fines content before compression

822

823 **Appendix A. Extrapolation of critical state**

824

825 The CSL is extrapolated by a four-parameter sigmoidal function proposed by Murthy et al. (2007). The  
826 function is expressed mathematically by

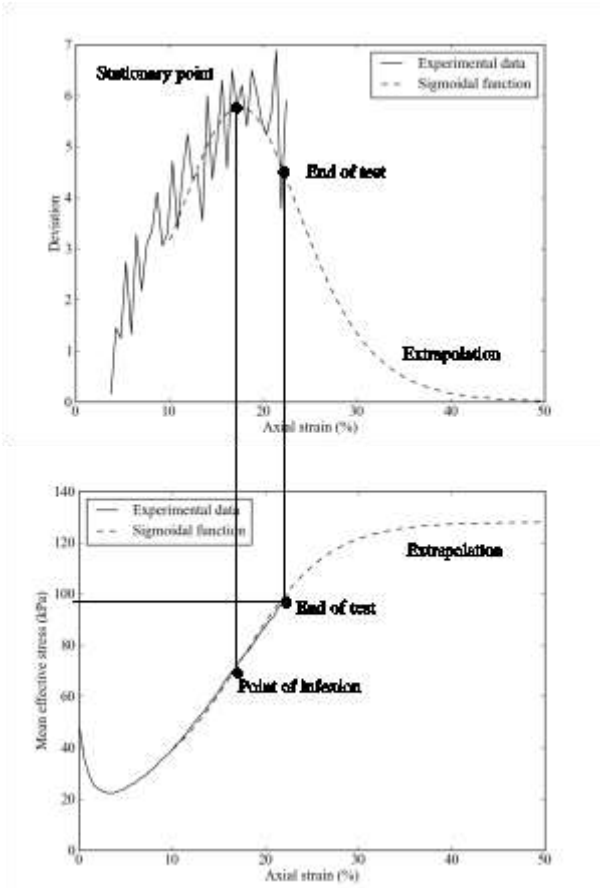
827 (a1) 
$$y = f(x) = a + \frac{b}{1 + e^{c(x-d)}}$$

828 where,  $a$ ,  $b$ ,  $c$  and  $d$  are the fitting parameters.

829

830 Initially, the curve of the first deviation of mean effective stress  $\partial p' / \partial \varepsilon_a$  against axial strain  $\varepsilon_a$  is  
831 plotted to find the stationary point, which is the projection of inflection in the relationship between  
832 axial strain  $\varepsilon_a$  and mean effective stress  $p'$ . Then, optimization was performed on both the  $\varepsilon_a - p'$  and  
833  $\partial p' / \partial \varepsilon_a - \varepsilon_a$  curves to get the fitting parameters of the sigmoidal function. To get the most reliable  
834 estimation of CSL, the global criterion method (Rao 2009) is utilized here. Figure A1 demonstrates the  
835 extrapolation process of the CSL of the uneroded soil containing 25% fines.

836



837

838 Fig. A1. Demonstration of the extrapolation of critical state

839